



Overview of recent ALICE results

Taku Gunji on behalf of the ALICE Collaboration

Center for Nuclear Study, the University of Tokyo, 7-3-1 Hongo, Bunkyo-ku, Tokyo, 113-0033, Japan

Abstract

The ALICE experiment explores the properties of strongly interacting QCD matter at extremely high temperatures created in Pb-Pb collisions at LHC and provides further insight into small-system physics in (high-multiplicity) pp and p-Pb collisions. The ALICE collaboration presented 27 parallel talks, 50 posters, and 1 flash talk at Quark Matter 2015 and covered various topics including collective dynamics, correlations and fluctuations, heavy flavors, quarkonia, jets and high p_T hadrons, electromagnetic probes, small system physics, and the upgrade program. This paper highlights some of the selected results.

Keywords: Quark-gluon plasma, Heavy-ion collisions, Jet quenching, Collective flow, Heavy flavor, Direct photons, Quarkonia, ALICE

1. Introduction

ALICE (A Large Ion Collider Experiment) is one of the major experiments at the CERN-LHC (Large Hadron Collider). ALICE is dedicated to the study of heavy-ion physics. The details of the ALICE detectors and performances in Run1 are described in Ref [1, 2]. The central features of the ALICE detectors are efficient charged particle tracking down to very low $p_T \sim 0.15$ GeV/c, excellent particle identification (hadrons, electrons, muons, and photons) over a wide momentum range, and excellent vertexing for the measurements of V^0 , cascades, heavy flavors, and conversion electrons from photons.

The ALICE collaboration has presented new and exciting results at Quark Matter 2015, which extend our knowledge on the dynamics of ultra-relativistic proton-proton and heavy-ion collisions. This paper is an overview of 27 parallel talks, 50 posters, and 1 flash talk delivered by the ALICE collaboration.

2. Highlights from Pb-Pb collisions

2.1. Collective Dynamics and Correlations

The first results on the p_T differential v_2 , v_3 , and v_4 for π^\pm , K^\pm , and $p + \bar{p}$ for top 0-1% and 20-30% centrality classes have been shown (upper panels of Fig. 1) [3]. These flow harmonics have been measured with the scalar product method with a pseudo-rapidity gap of $|\Delta\eta| \geq 0$ applied between the identified particles

¹A list of members of the ALICE Collaboration and acknowledgements can be found at the end of this issue.

and the reference charged particles. The contribution from non-flow effects is estimated using the HIJING event generator and corrected for. A clear mass ordering is seen in the low p_T region (for $p_T \leq 3$ GeV/c) for all v_n . The lower panels of Fig. 1 shows KE_T/n_q scaling for v_2 (left), v_3 (middle), and v_4 (right) for π^\pm , K^\pm , and $p + \bar{p}$ in 0-1% centrality. One can see that KE_T/n_q scaling works differently for different v_n and works best for v_3 .

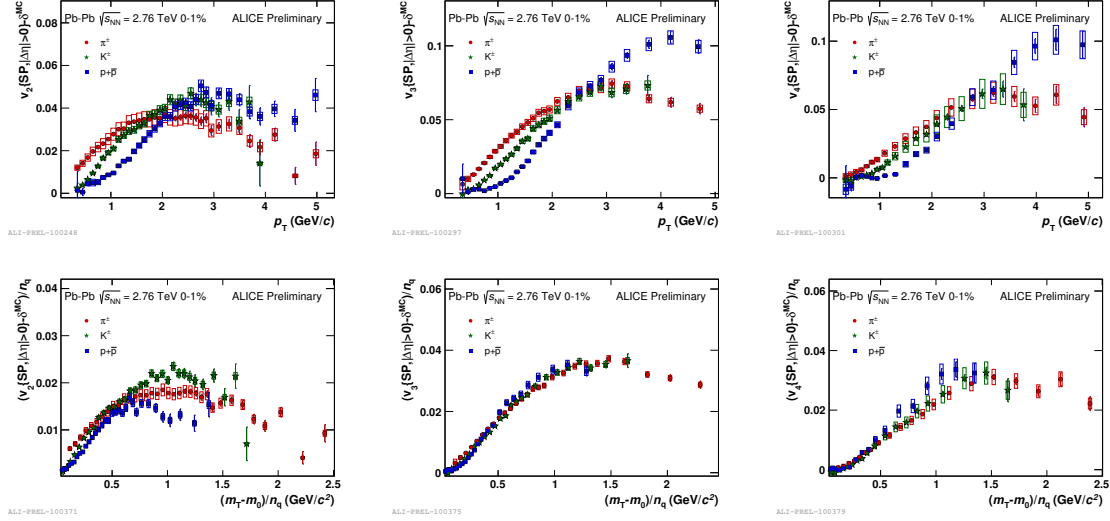


Fig. 1. (Color online) Upper: v_2 (left), v_3 (middle), and v_4 (right) for π , K , and protons in 0-1% centrality. Lower: KE_T/n_q scaling for v_2 (left), v_3 (middle), and v_4 (right) for π , K , and protons in 0-1% centrality.

Left and right of Fig. 2 show deuteron ($d+\bar{d}$), proton ($p+\bar{p}$), K^\pm , and π^\pm v_2 as a function of p_T in 10-20% and 30-40% centrality classes, respectively [4]. Solid lines are the results of the Blast-Wave model

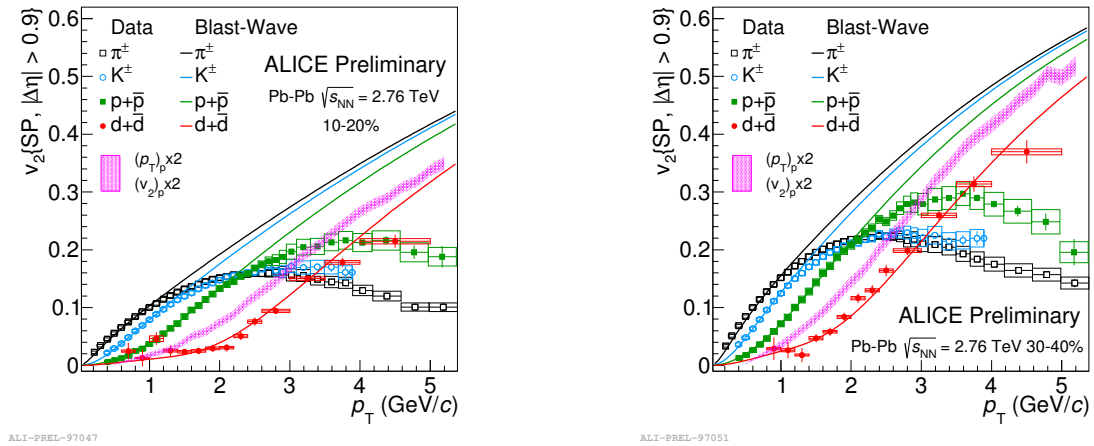


Fig. 2. (Color online) Deuteron v_2 as a function of p_T and v_2 expected from simple coalescence model for 10-20 % (left) and 30-40 % centrality (right).

fit to the measured π^\pm , K^\pm , and proton p_T spectra and v_2 . The deuteron v_2 is then calculated using the resulting Blast-Wave model fit parameters. Hatched area shows the p_T differential v_2 estimated by a simple coalescence model, where v_2 of deuteron is calculated as $v_2(p_T)_{\text{deuteron}} = 2v_2(2p_{T\text{proton}})_{\text{proton}}$. Deuteron v_2 is well-described by the Blast-Wave model and is overestimated by the simple coalescence model.

The first measurements of the correlations between different flow harmonics have been performed by using symmetric 2-harmonics 4 particles cumulants, which is defined as $SC(m, n) = \langle \langle \cos(m\psi_1 + n\psi_2 - m\psi_3 - n\psi_4) \rangle \rangle_c = \langle v_n^2 v_m^2 \rangle - \langle v_n^2 \rangle \langle v_m^2 \rangle$, where ψ is the azimuthal angle of particles. Figure 3 shows SC as a function of collision centrality, where boxes and circles correspond to $SC(4, 2)$ and $SC(3, 2)$, respectively [5]. Positive (negative) correlations are seen between v_2 and v_4 (v_3) and the correlations are not described by the HIJING generator (non-flow effects). These $SC(m, n)$ values are sensitive to shear viscosity/entropy ratio ($\eta/S(T)$) of the created medium, as is shown in the right panel of Fig. 3, where 4 sets of $\eta/S(T)$ parametrization are used for the comparison. While centrality dependence of charged particle $v_n\{2\}$ is described by this parametrization [7], SC measurements can provide stronger constrains on $\eta/S(T)$ than standard v_n measurements.

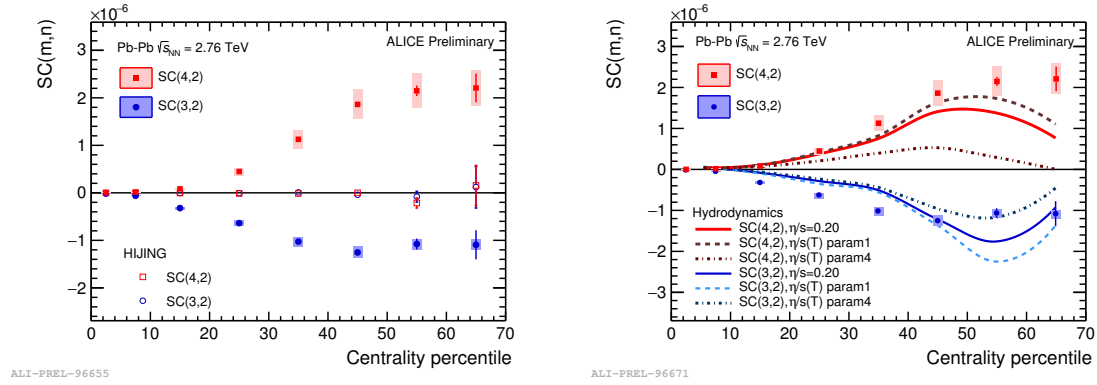


Fig. 3. (Color online) $SC(4,2)$ and $SC(3,2)$ as a function of centrality and comparison with HIJING with non-flow contributions (left) and hydrodynamical model calculations with different parametrization of $\eta/S(T)$.

2.2. Hard Probes

Heavy flavors (i.e. charm and beauty) and jets are important probes for studying the properties of the medium since they are produced in the initial hard scattering and interact with the medium over the full evolution. ALICE released new results on the nuclear modification factor (R_{AA}) of D and D_s mesons, R_{AA} and v_2 of forward muons from heavy-flavor semi-leptonic decays, charged jet v_2 , and modifications of jet-core shape inside near side jets [10, 11, 12, 13].

2.2.1. Heavy Flavors

Left of Fig. 4 shows R_{AA} for π^\pm , D , and non-prompt J/ψ measured in similar p_T ranges ($8 \leq p_T \leq 16$ GeV/ c for π^\pm and D and $6.5 \leq p_T \leq 30$ GeV/ c for non-prompt J/ψ) as a function of the number of participants. The D meson R_{AA} is much smaller than non-prompt J/ψ R_{AA} and is compatible with that of π^\pm within uncertainties. These two observations are simultaneously described by models accounting for mass-dependent energy loss ($\Delta E_g \geq \Delta E_{u,d,s} \geq \Delta E_c \geq \Delta E_b$), different shape of the parton p_T spectra and different parton fragmentation functions [14]. Right of Fig. 4 shows R_{AA} as a function of p_T for D and D_s mesons in 0-10% centrality. A hint of less suppression of D_s mesons for $p_T \leq 8$ GeV/ c is visible, which is attributed to the strangeness enhancement in the medium and dominance of coalescence process for D_s meson production.

2.2.2. Jet-core shapes

Three new observables are introduced and studied by ALICE to characterize the jet-core shapes: radial momentum ($g = \sum p_T^i |\Delta R_i| / p_{T,jet}$), dispersion in p_T , and difference in p_T between leading and sub-leading jet constituents. Left of Fig. 5 shows the radial moment distribution in 0-10% top central collisions and the comparisons with PYTHIA Perugia 2011. Right of Fig. 5 shows the comparison with JEWEL calculations with and without quenching and the quark and gluon jet core shapes estimated by PYTHIA Perugia

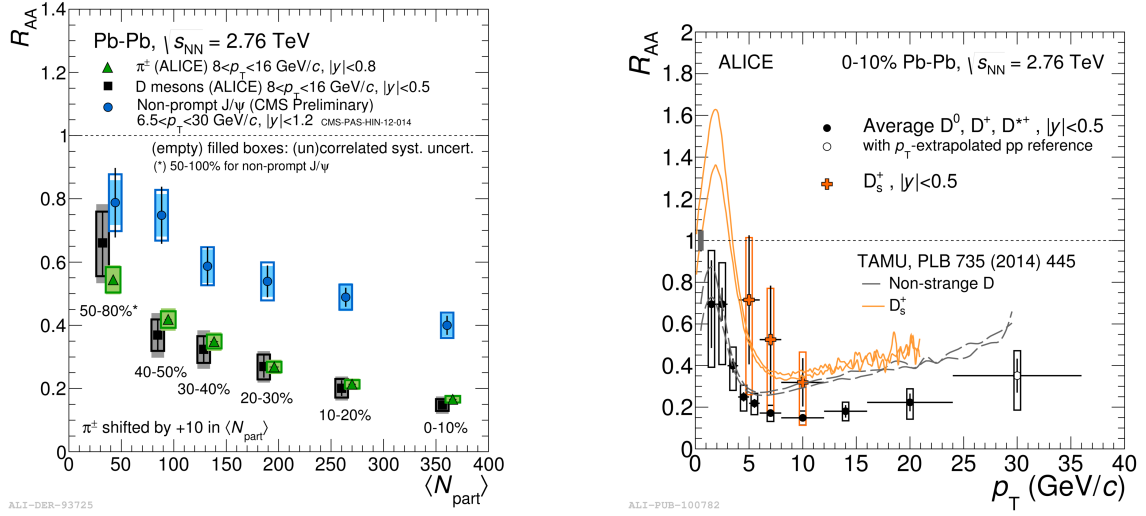


Fig. 4. (Color online) Left: R_{AA} as a function of the number of participants (N_{part}) for π^\pm , D , and non-prompt J/ψ at similar p_T range. Right: R_{AA} as a function of p_T for D and D_s mesons in 0-10% centrality.

2011. The radial moment distribution is shifted to lower values in Pb-Pb collisions when compared with pp collisions, which means that Pb-Pb jets are more collimated than pp jets. This collimation is described by JEWEL model calculations indicating that the measured jet quenching and jet shape favor quark jets rather than gluon jets. This result suggests that gluon jets are more quenched than the quark jets resulting in a change of the quark/gluon jet relative composition in Pb-Pb collisions.

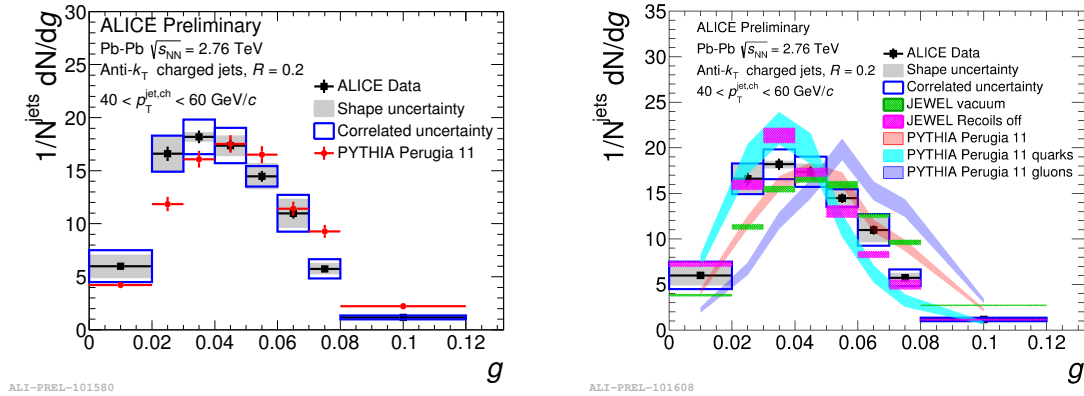


Fig. 5. (Color online) Left: Radial moment distributions of jet-core within $R = 0.2$ in Pb-Pb collisions and from PYTHIA Perugia 11. Right: Radial moment distributions of jet-core and comparison with JEWEL calculations with and without quenching and shapes from quark and gluon-jets calculated by PYTHIA Perugia 11.

2.3. Low p_T Photons

ALICE has measured the direct photon spectra in Pb-Pb collisions for three centrality classes by using the photon conversion method and the PHOS calorimeter [9]. A 2.6σ excess of low p_T photons above pQCD calculations is observed in central 0-20% collisions. The inverse slope parameter is extracted for 0-20% centrality and found to be $304 \pm 11^{stat} \pm 40^{sys}$ MeV, 30% larger than the slope measured at RHIC.

2.4. Longitudinal Asymmetry

When two nuclei collide, the number of participants for each one can be different due to the fluctuations of the nucleon density. These event-by-event fluctuations are estimated by measuring the asymmetry in the energy deposition in the two neutron ZDCs. The effect of these fluctuations on the $dN/d\eta$ distributions of charged particles has been studied for the first time. Left of Fig. 6 shows the distribution of the asymmetry in the energy deposition in the two ZDCs for 15-20% centrality class [15]. Events have been further classified based on the measured energy asymmetry, where Region-1, Region-2, and Region-3 covers $\alpha_{ZDC} = (E_{ZNA} - E_{ZNC})/(E_{ZNA} + E_{ZNC}) < -0.1$, $\alpha_{ZDC} > 0.1$, and $|\alpha_{ZDC}| < 0.1$, respectively. The ratio of the measured $dN/d\eta$ distributions for Region-1 to Region-3 (box) and Region-2 to Region-3 (circle) is shown in the right of Fig. 6. One can clearly see a shift of the measured $dN/d\eta$ distributions for the events in Region-1 and Region-2 [15]. Solid lines are the results of a fit to the ratios for both Region-1/Region-3 and Region-2/Region-3 with a cubic function. From the fitted coefficient, the values of the rapidity-shift is obtained and is found to be consistent with the estimations from a Glauber model calculation [15].

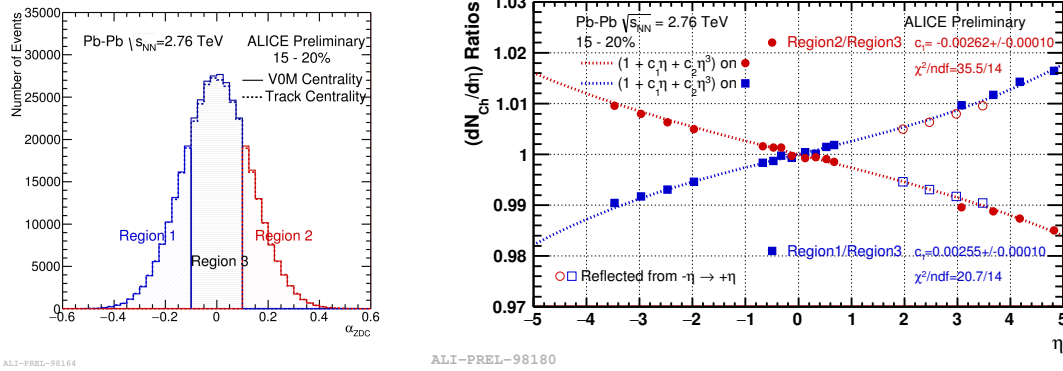


Fig. 6. (Color online) Left: Measured energy asymmetry between two ZDCs in ALICE. Right: Ratio of $dN/d\eta$ between different measured energy asymmetric events. (circle: region2/region3, open: region1/region3)

3. Highlights from pp and p-Pb collisions

Recent intriguing results in heavy-ion physics raised questions on the origin of the non-trivial effects observed in high-multiplicity pp and p-Pb collisions such as the behavior of $\langle p_T \rangle$ and identified particle spectra as a function of multiplicity [16, 17], long-range correlations [18], and mass ordering of v_2 [19]. ALICE presented new exciting results, which include quarkonia and heavy-flavor production [20, 21] and v_2 of forward muons in p-Pb collisions [22], and strangeness production (Λ , Ξ , Ω) in pp collisions [23].

3.1. Cold and hot matter effects

Left and right of Fig. 7 show the inclusive J/ψ [24] and $\psi(2S)$ Q_{pPb} as a function of the number of binary collisions at backward ($-4.46 \leq y_{CMS} \leq -2.96$) and forward ($2.03 \leq y_{CMS} \leq 3.53$) rapidities, respectively ². The centrality determination is based on the measured energy deposition in the two neutron ZDCs, which is the least biased estimator [25]. The J/ψ production is compatible with the binary scaling at backward rapidity, while at forward rapidity the J/ψ production is suppressed for all centrality classes. These trends are well-described by initial state effects such as gluon shadowing and initial state energy loss. The $\psi(2S)$ suppression is visible in both rapidity intervals and increases with the centrality, where the final state interactions with a comoving medium and in the hadrons resonance gas is needed to explain the observed $\psi(2S)$ suppression.

² Q_{pPb} is the centrality-dependent nuclear modification factor defined as the yield ratios in A+A and pp collisions scaled by the number of binary collisions. This notation is used to warn for possible biases in the determination of the number of binary collisions.

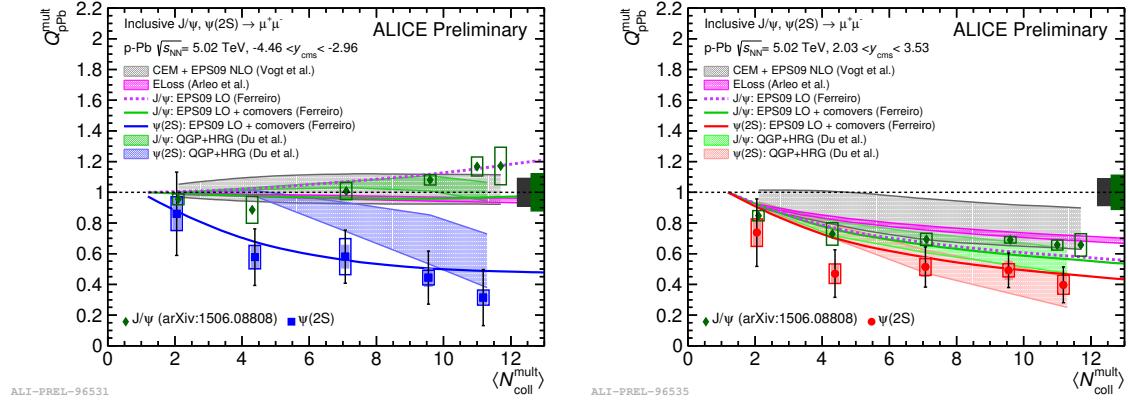


Fig. 7. (Color online) Q_{pPb} as a function of forward rapidity (p-going direction) (left) and as a function of backward rapidity (Pb-going direction) (right) and comparison with models.

3.2. Forward muon v_2 in p -Pb collisions

ALICE has measured long-range correlations at $\Delta\eta$ of up to 5 by taking the correlations between forward muons and midrapidity tracks or tracklets [22]. A double ridge structure is visible up to $\Delta\eta \sim 5$ and the extracted p_T differential v_2 of forward muons shows larger v_2 in Pb-going direction than in p-going direction, which is in accordance with AMPT calculations. It is found that v_2 of forward muons above 2 GeV/c, where 60% of muons are from heavy-flavor decays, is larger than zero.

3.3. Heavy flavor production vs. event multiplicity in p -Pb collisions

Left and right of Fig. 8 show the self-normalized yields of D mesons as a function of relative multiplicity based on two different multiplicity estimators, where one uses the number of tracklets in SPD at $|\eta| \leq 1$ and the other uses multiplicities measured with V0A (Pb-going direction) covering $2.8 \leq \eta \leq 5.1$. For the SPD estimator, the results exhibit a faster-than-linear increase in the relative D meson yields, while for the V0A estimator, the results show a roughly linear increase as a function of multiplicity up to the interval of $N_{V0A}/\langle N_{V0A} \rangle \leq 3.5$.

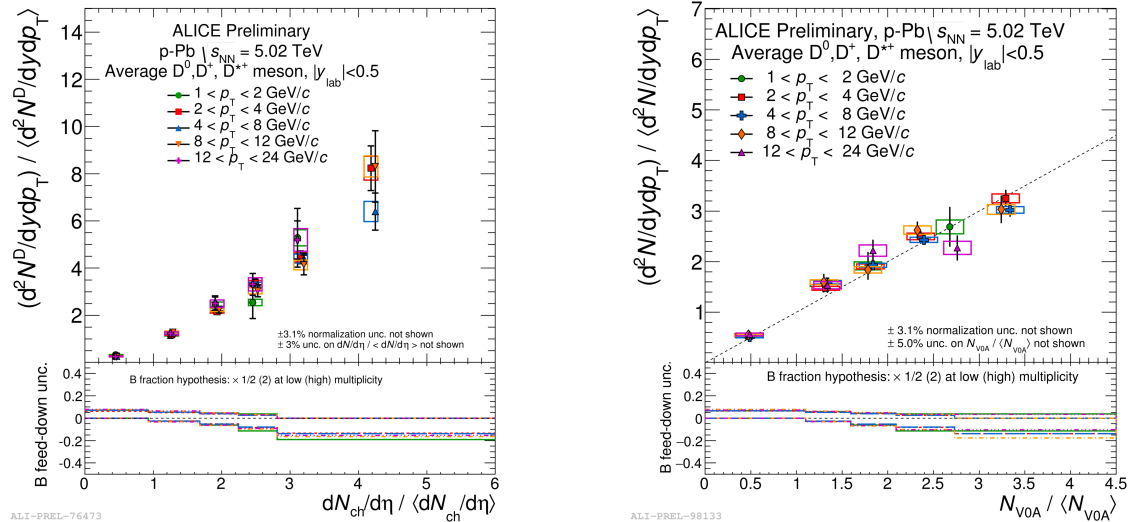
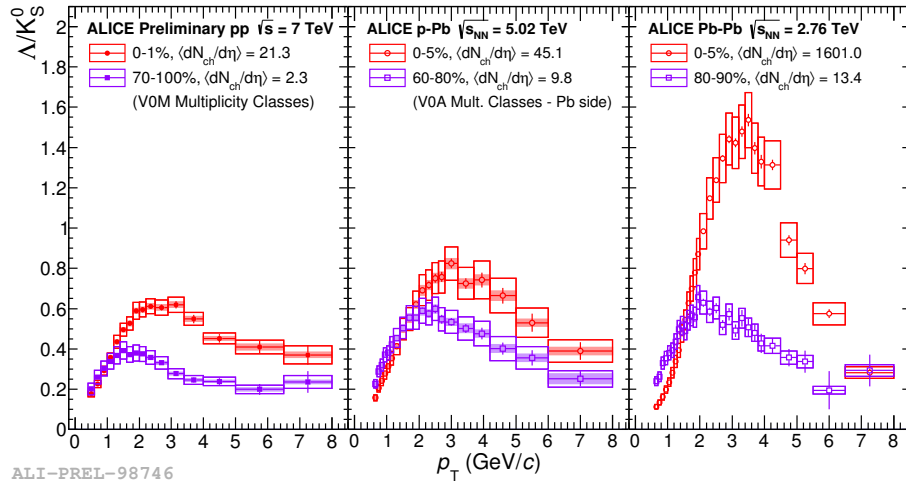


Fig. 8. (Color online) Self-normalized yield as a function of relative multiplicity in p -Pb collisions. Relative multiplicity is estimated by SPD tracklets (left) and V0 detector at forward rapidity (right).

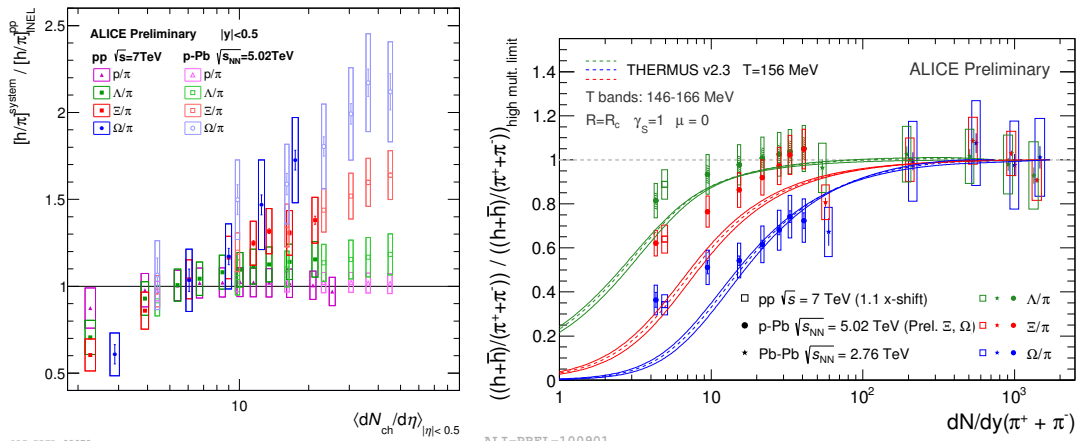
3.4. Strangeness production vs. event multiplicity in pp collisions

Figure 9 shows the p_T differential Λ/K_s^0 ratio in the highest and lowest multiplicity classes for pp (left), p-Pb (middle), and Pb-Pb (right) collisions. The ratio depends on the event multiplicity and the magnitude of Λ/K_s^0 is qualitatively similar in 0-1% pp, 60-80% p-Pb, and 80-90% Pb-Pb multiplicity classes, where the $\langle dN_{ch}/d\eta \rangle_{|y| \leq 0.5}$ value is also comparable. Left of Fig. 10 shows the yield ratios for proton, Λ , Ξ , and Ω to pion yields normalized to the values measured for pp INEL event class. Faster enhancement for $\Omega > \Xi > \Lambda$ is clearly visible, while the ratio for proton stays constant, and these trends are similar in pp and p-Pb collisions. Right of Fig. 10 shows the ratio to pions in pp, p-Pb, and Pb-Pb collisions normalized to the value in the highest multiplicity class in Pb-Pb collisions. Solid and dashed lines are the statistical model calculations and the decrease in the ratios is interpreted as due to the canonical suppression.



ALI-PREL-98746

Fig. 9. (Color online) $(\Lambda + \bar{\Lambda})/K_s^0$ as a function of p_T in the highest and lowest multiplicity classes in pp (left), p-Pb (middle), and Pb-Pb collisions (right).



ALI-PREL-98972

ALI-PREL-100901

Fig. 10. (Color online) Left: Multi-strangeness (λ , Ξ , Ω) and proton yield ratios to pions normalized to the values in pp 0-100%. Right: Multi-strangeness yields normalized by the yields in the highest multiplicity class in Pb-Pb collisions.

4. ALICE in Run2 and Prospects for Run3

During the Long Shutdown 1 of the LHC, the remaining five super modules of the TRD, eight modules of new dijet calorimeter (DCal), one module of PHOS, and new ALICE Diffractive detectors (AD) have been installed. ALICE Central Trigger Systems have been upgraded to handle 100 trigger classes. The gas mixture of TPC has been changed from Ne(90):CO₂(10) to Ar(90):CO₂(10), to provide a more stable operation in high particle fluxes during heavy-ion running. ALICE started taking data in pp collisions at $\sqrt{s} = 13$ TeV in June 2015. Charged particle multiplicities and p_T spectra for different multiplicity classes in pp INEL and INEL > 0 events are reported in Ref. [26].

The ALICE upgrades after Long Shutdown 2 (2019-2020) are focused on providing high precision measurements of dileptons, heavy flavors, quarkonia, jets and heavy nuclei with 100 times large statistics by taking minimum bias Pb-Pb collisions at 50 kHz [27]. Many activities of the various ALICE upgrades including ITS, TPC, Muon Forward Tracker (MFT), trigger and readout electronics, and new combined online-offline project are on-going [28]

References

- [1] K. Aamodt et al. (ALICE Collaboration), *JINST* **3**, S08003 (2008).
- [2] B. Abelev et al. (ALICE Collaboration), *Int. J. Mod. Phys. A* **29**, 1430044 (2014).
- [3] N. Mohammadi (ALICE Collaboration), Quark Matter 2015 Conference.
- [4] R. Lea (ALICE Collaboration), Quark Matter 2015 Conference.
- [5] Y. Zhou (ALICE Collaboration), Quark Matter 2015 Conference.
- [6] J. Adam et al. (ALICE Collaboration), arXiv:1507.06194; A. Timmins (ALICE Collaboration), Quark Matter 2015.
- [7] H. Niemi et al. arXiv:1505.02677.
- [8] K. Aamodt et al. (ALICE Collaboration), *Phys. Rev. Lett.* **107**, 032301.
- [9] J. Adam et al. (ALICE Collaboration), arXiv:1509.07324; B. Sahlmueller (ALICE Collaboration), Quark Matter 2015.
- [10] J. Adam et al. (ALICE Collaboration), arXiv:1506.06604, arXiv:1509.06888, arXiv:1509.07287, arXiv:1507.03134; A. Dubla (ALICE Collaboration), Quark Matter 2015.
- [11] J. Adam et al. (ALICE Collaboration), *JHEP* **07** (2015) 051
- [12] J. Adam et al. (ALICE Collaboration), arXiv:1509.07334; R. Alexander Bertens (ALICE Collaboration), Quark Matter 2-15.
- [13] L. Cunqueiro Mendez (ALICE Collaboration), Quark Matter 2015.
- [14] M. Djordjevic, *Phys. Lett. B.* **737** (2014) 298
- [15] R. Raniwala (ALICE Collaboration), Quark Matter 2015.
- [16] B. B. Abelev et al. (ALICE Collaboration), *Phys. Lett. B* **727** (2013) 371.
- [17] B. B. Abelev et al. (ALICE Collaboration), *Phys. Lett. B* **728** (2014) 25.
- [18] B. B. Abelev et al. (ALICE Collaboration), *Phys. Lett. B* **719** (2013) 29.
- [19] B. B. Abelev et al. (ALICE Collaboration), *Phys. Lett. B* **726** (2013) 164.
- [20] M. Leoncino (ALICE Collaboration), Quark Matter 2015.
- [21] J. Wilkinson (ALICE Collaboration), Quark Matter 2015.
- [22] J. Adam et al. (ALICE Collaboration), arXiv:1506.08032; E. Kryshen (ALICE Collaboration), Quark Matter 2015.
- [23] L. Bianchi (ALICE Collaboration), Quark Matter 2015.
- [24] J. Adam et al. (ALICE Collaboration), arXiv:1506.08808
- [25] J. Adam et al. (ALICE Collaboration), *Phys. Rev. C* **91**, 064905, 2015.
- [26] J. Adam et al. (ALICE Collaboration), arXiv:1509.08734
- [27] B. Abelev et al. (ALICE Collaboration), *J. Phys. G* **41** (2014) 087001
- [28] B. Abelev et al. (ALICE Collaboration), *J. Phys. G* **41** (2014) 087002; ALICE Collaboration, CERN-LHCC-2013-020; ALICE Collaboration, CERN-LHCC-2015-001; ALICE Collaboration, CERN-LHCC-2013-019; ALICE Collaboration, CERN-LHCC-2015-006; P. Riedler (ALICE Collaboration), Quark Matter 2015; C. Garabatos (ALICE Collaboration), Quark Matter 2015